Dear Editor Niemeijer, Dr. Aben and anonymous reviewer,

Thank you for these constructive reviews. We have significantly modified the abstract, introduction and discussion to more clearly specify the motivation and new contribution of this work. We respond to the comments point-by-point below in bold font. We added numbers to each point for clarity. We respond to the annotations of the manuscript by the anonymous reviewer in the attached document.

Thanks,
Jessica McBeck

Franciscus Aben (Referee)

The manuscript entitled 'The competition between fracture nucleation, propagation, and coalescence in the crystalline continental upper crust' by McBeck et al. aims to illuminate the nucleation, growth, and coalescence of micro-fractures in crystalline rock prior to sample-size shear failure, and how this 'road-to-failure' varies in the presence/absence of pore fluids. To do so, three shear failure experiments (2 dry, 1 saturated) were conducted in a triaxial vessel, whilst obtaining a full 3D X-ray tomography model at set intervals of differential stress up to sample failure. The 3D X-ray tomography data was analysed to obtain measures for microfracture nucleation, propagation, and coalescence. The main conclusion of the manuscript is that under fluid saturated conditions, microfractures tend to propagate more in isolation rather than coalesce with nearby microfractures relative to the dry case. This interesting conclusion based on the observations and excellent data analysis warrants publication, but the manuscript first needs to address a number of significant problems. These problems comprise the lack of clarity on the main aim of the manuscript, and a somewhat tedious discussion section with unclear/inconsistent arguments. I hope that my comments below will be of help to improve the quality and the originality of the manuscript.

Major comments:

1. The main aim of the manuscript is not clear: Is it the 'road-to-failure' with an additional step in the X-ray tomography data analysis (i.e., quantification of fracture coalescence), or is it trying to elucidate the difference in pre-failure deformation for dry and saturated conditions? This duality is making it difficult to follow, especially in the introduction and the discussion sections of the paper, and the authors may wish to rethink this. Moreover, the 'road-to-failure' has been studied and presented by (some of the) authors in other recent manuscripts, partly on the same dataset, and the additional data analysis step feels like a somewhat meager addition to these previous works. I feel that the observations on microfracture development with/without fluids does contribute more significantly to progressing our understanding of brittle rock deformation between the yield point and sample-scale failure, and so I recommend to emphasize this as the main aim of the manuscript (studied with the approach of measuring of fracture coalescence, propagation, etc.).

   We have significantly modified the introduction and underscored throughout the text that the central focus of the paper is quantifying the competition between nucleation, propagation and coalescence, and tracking how this competition changes throughout loading (toward failure) and in dry and saturated conditions (lines 9-15, 42-43, 57-58, 76-77, 194-195, 220-221, 223). None of our previous work (or other analyses that we are aware of) have quantified these different modes of fracture growth, which exert a significant impact on permeability and fluid-rock interactions. Therefore, the main outcome of the present study is the quantification of the dominance of nucleating, propagating, and coalescing fractures. The secondary outcome is

the difference of behaviour in the water-saturated sample compared to the two dry samples.

2. Following on this, the title does not cover entirely the content of the manuscript, and should contain some mention of the dry vs. saturated conditions.

   We have now modified the title as suggested.

3. I believe that (part of) the data has been presented in other manuscripts, so it should be clarified better what the innovative aspect is of this manuscript in relation to previous ones. Also, indicate which sample data sets have been presented in which manuscripts before.

   The three experiments have been described in Renard et al. (2018) (#3 and #4) and in Renard et al. (2019) (#5). However, the analyses presented here provide a fundamental advance from this previous work. The new data processing done here enables quantifying the growth mode of individual fractures following a stress step increase: 1) nucleation, 2) propagation of an existing fracture, 3) coalescence, and thus tracking the evolution of these three kinds of growth modes until system-size failure. We have now clarified how this work differs from previously published work (lines 85-90, 119-121). Please see response to comment #1 above also.

4. The methodology section 2.1 is very short and lacks some basic experimental information: What deformation rig was used, what is the voxel size, what was the axial loading rate, how was axial shortening determined, and how much time was allowed for the pore fluid pressure to equilibrate across the sample prior to the onset of loading, and in between load steps?

   We have now added this relevant information in Section 2.1.

5. Line 145: The authors may want to add some clarification on the meaning of nucleating fractures in their data: It seems to me that the fractures that appear within the resolution of the X-ray data at each step may have been there the previous step as well, only not detected due to their size/small volume. It is most likely that they nucleated from a preexisting defect (grain boundary, cleavage plane) that initially had no volume to begin with. This does not hamper the analyses here, but it would clarify that the term nucleation used here is somewhat relative to scale/resolution, and does not describe fractures forming out of the blue. This brings up the interesting point as well on what is actually measured: The volume of microfractures. Do the authors think there are many 'hidden' pure shear microfractures without much opening (i.e., volume) in their data?

   We have now added the important point that the identification of nucleating fractures depends on the scan voxel size, and the identification of all of the fractures depend on their opening (lines 159-162). It is difficult to make a quantitative statement about potential hidden fractures, and thus the proportion of shear vs. dilation. Early studies, such as Tapponier & Brace (1976), observed few shear fractures in their data, and now we mention this good point in the discussion (lines 308-309).

6. The authors attempt to explain coalescence from a linear elastic fracture mechanics perspective, with the hypothesis that fractures near each other are more likely to grow because their fracture tip stress concentrations interact. This is introduced first in section 3.4, and further expanded upon in section 4.4. This hypothesis is not well

explained or quantified: It seems to me that such an interaction depends on the length of the fractures involved (longer fractures, larger stress intensity) and on their orientation, as well as on the exact stress fields around them (e.g., mode-II fractures have reduced and increased stresses near their tip, whereas mode-I fractures do not). So I am not sure if I understand well or agree with line 208: 'The observations match the expectations of LEFM'. Secondly, contrary to this hypothesis is the statement in the introduction that LEFM cannot explain well fracture coalescence (line 30-35), so why choose this as a framework to explain the observations on coalescence?

In the introduction, we have modified the text to specify that "such analytical formulations struggle to describe the coalescence behavior of fracture networks as they transition from distributed, disperse networks comprised of many isolated, small fractures to more localized networks comprised of well-connected, larger fractures. This transition includes a continuum of fracture development that may be divided into three endmember fracture growth modes: 1) nucleation, 2) isolated propagation and 3) coalescence." (lines 37-41).

Although these analytical formations struggle to describe coalescence, they can provide insights into the potential propagation of individual fractures, and how this depends on the fracture's length, orientation and stress fields (as mentioned by the reviewer). Thus, examining the extent of the agreement between these LEFM predictions (stress intensity factor) and the experimental results is useful. We agree that the stress intensity factor is controlled by the fracture length, orientation and surrounding stress field. Precisely because fracture length controls the stress intensity factor, it also controls the local stress perturbation produced by the fracture. For this reason, analytical formations suggest that fractures perturb their local stress field to a distance on the order of their length (e.g., Scholz et al., 1993). However, the nature of this perturbation can promote or hinder fracture growth depending on the loading conditions and fracture network geometry. We have now modified the text in the results, discussion and conclusion to more clearly describe this point and how our data indicate how fractures promote or hinder the growth of neighbouring fractures (lines 226-228, 241-243, 247-248, 373-375, 395-396).

7. Section 4.2 discusses the competition between fracture nucleation and isolated propagation. This is somewhat tedious because the authors elect to use the analogy of sandstone deformation and models designed for layered sedimentary sequences for crystalline low porosity rock. I do not feel this is very informative: Triaxial deformation of granular aggregates is very different from low porosity rock, and the step from a small-sized crystalline rock sample to a sedimentary basin feels like a leap. Most discussion is summarized in the last paragraph of this section: This competition seems adequately explained by the fracture length dependent stress intensity factors, so that a few growing fractures shield shorter (nucleating) fractures. As a suggestion, the authors could analyse the lengths of the fractures in loading-parallel direction in their data to provide a somewhat more quantitative argument here.

   We agree that aspects of the micromechanisms that operate in granular aggregates differ from that of low porosity crystalline rock. We note in the text that "Granular rocks may contain mechanical heterogeneities that concentrate shear and/or tensile stresses more effectively than monzonite, which consists of an interlocking crystalline structure with relatively homogeneous mechanical properties." (lines 268-270). However, fracture development is

similar in these rock types in that "mechanical heterogeneities control the location of fracture nucleation and the growth of preexisting fractures." (lines 258-249). Because nucleation is linked to stress concentrations, discussion of the factors that produce stress concentrations seems germane to this paper. We have rewritten parts of the discussion to emphasize the links between the different rock types (lines 275-276, 285-286, 304). We have also removed the previous Section 4.1 to improve the conciseness and focus of the discussion.

We note that in the reviewer's JGR 2020 paper (Aben et al., 2020), the authors also link experiments on low porosity crystalline rock to deformation mechanisms in porous rocks in the discussion section: "Porous rock such as sandstone is known to collapse at high hydrostatic pressure (e.g., Wong & Baud, 2012), and a similar type of local pore collapse may also occur in pulverized rock". We also follow this approach of linking mechanisms between various rock types when it is justified.

Aben, F. M., Doan, M.-L., & Mitchell, T. M. (2020). Variation of hydraulic properties due to dynamic fracture damage: Implications for fault zones. Journal of Geophysical Research: Solid Earth, 125, e2019JB018919. https://doi.org/10.1029/2019JB018919

8. I feel that Section 4.3 contains some similar problems as discussed above: The sandstone analogy is not a very helpful argument to explain competition between isolated fracture propagation and fracture coalescence in crystalline rock, and neither is fault damage zone evolution: The presented data is on an initially intact sample without a pre-existing fault zone. Further irrelevant excursions include the 316-318 on dilation in gouge materials.

   In these discussion sections, we try to be careful to address the differences between the experiments analysed here and the previous work. The link between the current work and studies with sandstone and damage zones is that "observations indicate that the magnitude of confining stress influences fracture development" (line 306). Our general view is that rock deformation analyses benefit from reasonable generalization between different rock types, rather than only narrowly focusing on one rock type. Similarly, we included the description of dilation within gouge material in the section on dilatant hardening because gouge-filled fault zones are another system with dilatant hardening operates. We have rewritten portions of the discussion to improve conciseness.

9. Section 4.3 contains, in my opinion, the most interesting discussion: The influence of fluids on microfracture evolution prior to sample-sized failure. The authors first discuss the different confining pressures on all three samples as the source for the different microfracture evolution, and rule this out as a conclusion. Second, the chemical effect of water on crack propagation is discussed, followed by a discussion on the mechanical effect of a pressurized fluid. The authors conclude, rightly so, that these last two effects cannot be distinguished from each other and future research is necessary. I largely agree with the line of thought and the conclusion of the authors, but there are a few caveats and/or additional points that need to be addressed, starting at the level of the experiment: How does the sample size (4x10 mm) influence the reproducibility of the experiments, especially given the relative large (450um on average) grain size of the material (for instance, some grains seem to have dimensions of > 1mm in the 3D CT models)? Secondly, dilatancy hardening is presented as a mechanism to influence microfracture evolution, but how specifically is not clear. Dilatancy is often discussed on the scale of cm-size (and larger) shear

fractures or fault planes, where fault roughness and microfractures around the shear plane accommodate the dilation. Here, the microfracture regime does not yet have such a centralized structure, but could it be possible that larger and coalescing microfractures have a larger dilatancy rate than smaller fractures, so that the former are more affected by dilatancy? On stress corrosion: The authors could try to include a back of the envelop calculation on how long it takes for fluids to reach the crack tips during and after a deformation step – i.e., are the crack tips wetted during propagation, and has the pore fluid pressure equilibrated within the sample? I have measured hydraulic properties on these monzonites that may prove helpful to measure diffusion times. ("Variation of Hydraulic Properties Due to Dynamic Fracture Damage: Implications for Fault Zones", JGR 2020)

Indeed, we are also curious about the reproducibility of the results, and how grain size influences potential inconsistencies. Several features are reproducible in the three experiments such as the (power law) increase of fracture volume when approaching failure. The general trends of fracture development in the present study show also that the three samples do have a similar behaviour. So, we are confident that the results are robust. We observe a variation in this behaviour for the sample that contains water (i.e., Figures 4-6). We now are careful to note that our conclusions rest on only three experiments (lines 332-335, 356-358). Experiments planned for this fall will explore a wider range of confining stresses to address this point.

The question of the appropriate size of the representative elementary volume (REV) in this system is critical to address but difficult to estimate. Whether or not a REV exists depends on the rheology: for elastic materials it may exist, but for softening materials it may not (*Gitman et al*., 2007). Due to the large grain size of the monzonite relative to the core, we are close to the minimum limit of a REV in granular materials (10 grains), and far below an upper limit for stick-slip phenomena with glass beads (10^7) (*Evesque & Adjemian*, 2002). We now mention this good point in the text (lines 97-105).

Dilatancy hardening has also been observed in laboratory-sized samples, and not only systems with well-developed fault zones (e.g., *Brantut*, 2020).

We have now modified the text following the reviewer's good suggestion to calculate the length of time for fluid to flow across the rock core based on the porosity, and porosity-permeability calculations of Aben et al. (2020) (lines 347-356).

Gitman, I. M., Askes, H., & Sluys, L. J. (2007). Representative volume: existence and size determination. *Engineering fracture mechanics*, *74*(16), 2518-2534.

Evesque, P., & Adjemian, F. (2002). Stress fluctuations and macroscopic stick-slip in granular materials. *The European Physical Journal E*, *9*(3), 253-259.

10. Maybe I have missed it, but I could not find an in-text reference to Figure 7.

    This figure is referenced in the conclusion, and now we reference it in the discussion as well.

11. I feel that there is some overlap in the discussion at the end of section 3.4, and the discussion on LEFM and coalescence in section 4.4. Consider cutting the part in section 3.4.

We prefer to maintain this part of section 3.4 because the link between the analysis and the expectations of LEFM may require explanation in both places.

12. Line 31-32: I do not think this statement is correct: LEFM is scale-independent.

    We have rewritten this section of the introduction.

13. Line 38: Successful in what?

    We have rephrased the sentence for clarity (line 46).

14. Line 40: Clarify what is meant with the mode of failure.

    We have removed this sentence as it was extraneous.

15. Line 60-61: Does this not depend on whether the reaction is diffusion or precipitation controlled?

    We have rephrased the sentence accordingly (line 66-68).

16. Line 108: The fractures have been simplified as ellipsoids, how realistic is this shape, especially for coalesced fractures?

    For these monzonite rocks, the ellipsoidal shapes provide close approximations of the fracture geometry (i.e., Figure 1). For rocks like sandstone or marble where the grain boundaries exert a greater influence on fracture development, this approximation is further from the true shape. We have modified the text to address this good point (lines 138-140).

17. Line 122: In the description of how fractures are tracked from one X-ray dataset to the next, would it be clearer to speak of fracture volume instead of fracture?

    Following comment #5, we have specified that the volume (and dilation) of the fracture is critical to identifying it in the tomogram (Section 3.4). In other words, we only identify volumetric fractures, and so “fracture volume” and “fracture” are synonymous in this context.

18. Line 126: Insert ’to’ in between step and those.

    Corrected as suggested.

19. The figure references are somewhat chaotic: I would refrain from referring to the figures until the results section, and not refer to results figures in the introduction.

    The end of the introduction section provides a brief summary of the analysis, including the loading conditions. And thus referencing Figures 1 and 2 here seems appropriate and helpful to the reader.

20. Line 138, line 227: The term elastic is not correct here, because unloading at this point would not reproduce the near-horizontal stress-strain curve.

    We agree and have removed this term.

21. Section 3.1: How did the samples look like post-failure? Did they exhibit a single shear fracture at a 30-degree angle to the loading axis?

    Two samples (#3 and #5) were completely crushed following macroscopic failure and so we could not recover them for further observations. For experiment #4, several scanning electron microscopy images were acquired after macroscopic failure. These images showed that one main fault, or series of connect fractures, oriented at ~30° from σ_1 formed (see Figure 4 c-d in Renard et al., 2018). We now mention this point in the text (lines 175-178).

22. Line 147: Do I understand correctly that nucleating fractures from a previous load step are counted as propagating fractures in the next step (i.e., the nucleation counter is set to zero)?

    Correct.

23. Line 150: Repetition from section 2, can be removed.

    Removed as suggested.

24. Line 159: Was the volume of fluid expulsed from the pore pressure pumps measured? If so, do they match with the volume increase inferred from microCT?

    We did not record the fluid expulsed from the pumps. This lack of recording was a limitation of the software that controls the HADES rig that we have now modified. For the next experiments with fluid pressure, we will record both the fluid pressure and the volume in the two pumps that independently control the pressure and flow at the inlet and outlet of the sample.

25. Line 165: Are the exponents of the increase comparable between all three samples?

    We have now included this result in the manuscript (lines 201-203).

26. Line 170: develop a ! used our developed (the method was already explained in section 2).

    We prefer to shortly describe the method here in case a reader skips the methods section.

27. Paragraph 184-196: The technical part of how to define near and distant fractures should move to the method section. Also, how were closing and growing fractures defined?

    Please see response to previous comment.

28. Line 217: in during -> in.

    Corrected as suggested.

29. Line 322: The word ‘analyses’ in this context suggests some calculations/ quantification. Maybe ‘Discussion’?

    Here, we mean to refer to the analyses presented in the results (and the corresponding quantification), and not only our discussion.

30. Figure 4: Would it be possible to indicate the four deformation stages here? Showing the fracture volume in mm3 instead of voxels would make it easier for readers to extract dilation rates. In panel (c), would it be possible to have the same scale, so that the logarithmic trends are easily comparable (also for figure 5b)?

    Showing the 4 stages produces rather cluttered figures, so we prefer to only show the yield point on these figures. As 1 voxel is 6.5^3 μm^3, the dilations are readily calculated using these units. We have reformatted this figure so that the plots in c) have the same scale. We also now show the fits of the exponential functions of the propagating fractures in b), from which we calculated the exponents (see comment #25).

31. Some referencing is incomplete or skips over classic papers: line 28: The development of microfracturing with stress was already well documented by earlier studies than those cited here, especially from the 70s onward. For instance, Tapponier & Brace, 1976 have performed excellent microstructural work on this (see Paterson and Wong, section 5.7.4, for more refs).

    We have now added additional references in the introduction (line 33-35) and throughout the text.

32. Line 223-224: This statement is not correct: mechanical data, AEs, and microstructures show the development of microfracture networks past the yield point; Brace, Paulding, and Scholz 1966 inferred microcracking to be responsible for significant pore volume change during loading; Tapponier & Brace, 1976 and Wong 1982 show microstructures; AEs by Scholz 1968. These are examples of the older, more classic works that show this.

    We agree that AE data and microstructural data acquired after loading support this idea. **We have now modified the discussion by removing the section that contained this sentence. This discussion section did not significantly add to this contribution, and so we removed it for conciseness.**

33. Line 316: Martin III, 1980 ("Pore pressure stabilization of failure in westerly granite") may be more relevant here, as it shows the phenomenon in crystalline rock.

    We have now added this very relevant reference.

Review #2

The manuscript "The competition between fracture nucleation, propagation and coalescence in the crystalline continental crust" by Jessica A McBeck, Wenlu Zhu, and Francois Renard addresses the controls of development of fracture networks. McBeck et al. present an experimental study in which the fracture network development was assessed via microtomography during triaxial mechanical tests on two dry and one water-saturated sample. The data they acquired is remarkably and the method provides a great example of how fracture networks can be tracked during loading. The main outcome, that stress state and saturated vs dry conditions of the sample are the main controls of which (endmember) fracture network develops on the way to macroscopic failure, is not reflected in the title, introduced, clearly highlighted in the methods, represented in the results or adequately discussed. The authors need to address all of the following issues so the community can appreciate the scientific contribution.

34. The main message of the manuscript is not clear. It is not clear if they want to highlight the methodological approach or the results they obtained by applying the

method. The research question for this paper though is well hidden. The scope of the manuscript, the objectives and hypothesis are not clear.

We wish to highlight both the methods and the results. We have significantly modified the abstract, introduction, and discussion to highlight the research questions more clearly. We also now state that the main scientific question relates to the tracking of the mode of propagation of microfractures (see answer to comment #35 below). A secondary result is the effect of pore pressure.

35. It is not clear what the motivation for these experiments was. Data seems to be the same as in previous publications, which is fair to use as getting proposals funded and time allocated to do the experiments can be difficult, but it needs to made clear, where this data is new and where (re)used. 3. In the introduction, the overall concept of how fracture networks develop is not clearly outlined, thus that all assumptions and reasoning is vague. References are missing in many parts, which would allow substantiating some of the party awkward assumptions. The controlling variables which are used in the experiments and seem to be the main outcome are not introduced at all (effect of stress on fracturing, interstitial fluids).

    Although the data has been described in other papers, the new contribution of this work is the method for tracking fractures such that we may classify them as nucleating, propagating or coalescing. We describe this point in the methods section 2.3 and in the introduction (lines 85-90, 144-146). We have expanded this point in the introduction section.

    The central characteristics of fracture network growth that we focus on in this work include the three categories of development that are described in the first sentence of the introduction, and listed in the title. There are many aspects of fracture network growth outside of the purview of this analysis that we did not describe. We have significantly modified the introduction to clarify our use of the term mode.

    We discuss the influence of confining stress and fluids in the discussion section in depth.

36. The methods do not introduce the techniques applied both the mechanical loading (e.g. rate of loading) and the tomography (e.g. which voxel size), as well as how you analyse the data (e.g. volume calculation, attribution to which mode).

    We have added these important points to the Method section 2.1. We also now describe more specifically the two other studies that described these experiments.

37. The material used is not introduced at all. No description of the microstructure, no material properties (e.g. porosity). This makes it impossible to relate the tomography images and fracture network development to anything. The nucleation and propagation, especially at lower stress steps will be at grain boundaries and pre-existing defects and flaws.

    We have added these important points to the Method section 2.1.

38. The first part of the results seems to belong to the methods, yet it is not clear which point is made. The description and representation of the results are hard to follow

and do not seem to grasp/show important information. For example, you could colour the “new” fractures and the ones that coalescence in the shown steps differently.

We assume that the reviewer is referring to section 3.1., which describes the macroscopic mechanical behaviour of the experiments. This behaviour is a result, and a method.

Assuming that the reviewer is referring to Figure 1, the 3 cores shown at the bottom of the figure are from the three difference experiments, and not from different steps of the same experiment. We now mention this point specifically in the caption.

39. The structure of each section is flawed. The wording is unclear. Logical jumps make it very hard to follow the text. Especially in the introduction, the methods and results.

    We have worked to improve wording and logic.

40. Most parts of the discussion seem to be about something completely different than the experiment (upscaling- from 10mm to upper crustal) or research question (I am assuming crystalline rocks – yet the discussion is on sedimentary basins). The development of the fracture network is not discussed. References, if given, do not fit the topic.

    Please see response to comments #7-8 above.

41. The conclusion is contradicting the introduction in several aspects (e.g. LEFM) and is tedious as it simply repeats some statements made before which are not substantiated in the manuscript.

    We have now modified the conclusion for conciseness.

42. Detailed comments: I have commented on the manuscript in detail for the Abstract and the Introduction (see supplement .pdf). The extent of these comments highlight some of the main issues of the manuscript and are alike for the following sections. The Figures are not fitting the manuscript or provide a visualization to enhance the text, some detailed comments can be found there.

    We have responded to all of the annotated comments in the attached document. We describe how we have modified the text in response to these comments as well.

    Figure S1:
    - "vox" –> "voxel" - The variation in fond size and labelling position is a bit irritating. Could you work on it? - what does this # refer to? why #3, #5 and then #4. Maybe add to caption what the three panel show. - log scale hardly visible -consider using a different symbol/colour for this type to clearly distinct from the nucleation, above. - Caption: This figure does not show this. It only shows it in comparison to another figure Please name which figure this relates to. -Caption: The main trends are not indicated (in figure or text) - what are they? To make the point, you could add the trends of the 100 voxels to the figures.

    We have reformatted this figure to improve clarity.

    The # refers to the experiment code number. The experiments are ordered in the figures as #3, 5, 4 because this order reflects the different loading

conditions. From experiment #3, 5, 4, differential stress and effective stress both increase, as stated in the caption to this figure. We are careful to include the loading conditions and fluid pressure with the # notation in all of the figures.

The main trends are described in the results section of the main manuscript: i.e., Figure 5, Figure 6. We now reference these figures in the caption of Figure S1.

Figure S2: -Again, fond size and labelling position are a bit irritating. Why did you change the colour scheme? -Why is this yield (point) line in red, while in a) they are in the same colour as the other lines

We have reformatted this figure to improve clarity. We have changed the color of the yield lines to red everywhere.

The competition between fracture nucleation, propagation and coalescence in dry and water-saturated crystalline continental upper crust

Jessica A. McBeck[1], Wenlu Zhu[2], François Renard[1,3]

[1]Njord Centre, Department of Geosciences, University of Oslo, Norway
[2]Department of Geology, University of Maryland, College Park, U.S.A.
[3]University Grenoble Alpes, University Savoie Mont Blanc, CNRS, IRD, IFSTTAR, ISTerre, France

Correspondence to: Jessica McBeck (j.a.mcbeck@geo.uio.no)

Abstract. The continuum of behavior that emerges during fracture network development may be categorized into three endmember modes: fracture nucleation, isolated fracture propagation, and fracture coalescence. These different modes of fracture growth produce fracture networks with distinctive geometric attributes, such as clustering and connectivity, that exert important controls on permeability and the extent of fluid-rock interactions. To track how these modes of fracture development vary in dominance throughout loading toward failure, and thus how the geometric attributes of fracture networks may vary under these conditions, we perform in situ X-ray tomography triaxial compression experiments on low porosity crystalline rock (monzonite) under upper crustal stress conditions. To examine the influence of pore fluid on the varying dominance of the three modes of growth, we perform two experiments under nominally dry conditions and one under water-saturated conditions with 5 MPa pore fluid pressure. We impose a confining pressure of 20-35 MPa and then increase the differential stress in steps until the rock fails macroscopically. After each stress step of **1-5 MPa** we acquire a three-dimensional (3D) X-ray adsorption coefficient field from which we extract the 3D fracture network. We develop a **novel** method of tracking individual fractures between subsequent tomographic scans that identifies whether fractures grow from the coalescence and linkage of several fractures or from the propagation of a single fracture. **Throughout loading in all of the experiments, the volume of preexisting fractures is larger than those of nucleating fractures, indicating that the growth of preexisting fractures dominates the nucleation of new fractures**. Throughout loading until shortly before failure in all of the experiments, the volume of coalescing fractures is smaller than the volume of propagating fractures, indicating that fracture propagation dominates coalescence. Immediately preceding failure, however, the volume of coalescing fractures is at least double the volume of propagating fractures in the experiments performed at nominally dry conditions. In the water-saturated sample, in contrast, although the volume of coalescing fractures increases during this stage preceding failure, the volume of propagating fractures remains dominant. The influence of stress corrosion cracking associated with hydration reactions at fracture tips and/or dilatant hardening may explain the observed difference in fracture development under dry and water-saturated conditions.

1. Introduction

Fracture and fault networks develop through the nucleation of new fractures, the propagation of new and preexisting fractures, and the coalescence of neighboring fractures (e.g., ***Tapponnier & Brace*, 1976; *Nemat-Nasser & Horii*, 1982; *Atkinson*, 1984; *Olson*, 1993; *Lockner et al.*, 1991; *Reches & Lockner*, 1994; *Martin & Chandler*, 1994; *Kawakata et al.*, 1997;** *Mansfield & Cartwright*, 2001; *Crider & Peacock*, 2004; *Jackson & Rotevatn*, 2013). Formulations of linear elastic fracture mechanics (LEFM) can describe the potential of propagation of one or a few fractures within linear elastic material (e.g., *Griffith*, 1921; *Irwin*, 1957). **However, such analytical formulations struggle to describe the coalescence behavior of fracture networks as they transition from distributed, disperse networks comprised of many isolated, small fractures to more localized networks comprised of well-connected, larger fractures. This transition includes a continuum of fracture development that may be divided into three endmember modes of fracture growth: 1) nucleation, 2) isolated propagation and 3) coalescence**.

The aim of this work is to provide experimental constraints on the stress and fluid conditions that promote the dominance of one mode of fracture network development over another. Identifying which of these modes dominates the others under varying conditions may be critical for accurate assessment of fracture network development. For example, if nucleation is the dominant mode of fracture development rather than isolated propagation, then using metrics that identify sites of potential fracture nucleation may be more **accurate** than using metrics that predict the conditions under which a preexisting fracture will grow. Metrics that indicate regions in which fractures may nucleate include the strain energy density, maximum Coulomb stress, maximum magnitude of shear stress, and highest tensile stress or least compressive stress (e.g., *Jaeger et al.*, 1979; *Atkinson*, 1987; *Du & Aydin*, 1993). Previous analyses have used some of these metrics to predict the direction of fracture growth from a preexisting fracture tip (e.g., *Olson & Cooke*, 2005; *Okubo & Schulz*, 2005; *Fattaruso et al*., 2016). However, these metrics can lead to conflicting predictions about both the sites of new fracture nucleation and the direction of fracture growth (e.g., *Madden et al*., 2017; *McBeck et al*., 2017, 2020). If preexisting fracture propagation is the dominant mode of development rather than fracture nucleation, then metrics that determine the conditions under which preexisting fractures will grow, such as the critical stress intensity factor (*Isida*, 1971), and the direction of fault growth, such as Coulomb shear stress, tensile stress, and energy optimization (e.g., *Pollard & Aydin*, 1988; *Müller,* 1988*; Mary et al*., 2013; *Madden et al*., 2017; *McBeck et al*., 2017), may provide more accurate predictions of fault network development than nucleation criteria. **Thus, determining which mode dominates deformation under varying confinement and fluid conditions may help identify analyses suitable for successful prediction of fracture network development.**

The mode of fracture growth that dominates deformation may also influence the permeability of the network and effectivity of fluid-rock interactions because these modes can control the connectivity, tortuosity, and total fracture surface area of the network (e.g., *Hickman et al*., 1995). In particular, if a fracture network is dominated by many isolated fractures that propagate independently, it may host lower connectivity, greater tortuosity, and higher fracture surface area available for chemical reactions than a network dominated by several connected fractures that form via

coalescence. The connectivity, tortuosity, and available fracture surface area may influence the effective permeability, and rate and extent of fluid-rock interactions (*Hickman et al*., 1995; *Blanpied et al*., 1998; *Lamy-Chappuis et al*., 2014; *Frery et al*., 2015). In particular, fluid-rock interactions in the rock with many distributed small fractures that hosts greater fracture surface area may be more effective than in one with a few large fractures with lower surface area, depending on the permeability of the rock and whether the reaction is diffusion-controlled (e.g., *Renard et al*., 2000). A distributed fracture network comprised of many unconnected fractures may produce lower permeability than a more localized and connected fracture network. This difference in permeability may then influence the ability of fluid to access rock surfaces and react with them. In turn, reactions that dissolve the host rock or precipitate new material can influence the porosity and permeability (e.g., *Sausse et al.,* 2001; *Tenthorey et al*., 2003; *Lamy-Chappuis et al*., 2014). Thus, identifying the conditions under which coalescence or isolated propagation dominates may help assess the efficiency of geothermal energy and unconventional fossil fuel productions, and identify sites ideal for waste disposal or CO_2 sequestration (e.g., *Saeedi et al*., 2016; *Cui et al*., 2018).

To investigate the relative contributions of the three endmember deformation modes to fracture network development, we quantify the evolution of 3D fracture networks in monzonite rock samples undergoing brittle failure using in situ dynamic X-ray synchrotron microtomography. We conducted three triaxial deformation experiments at room temperature and confining pressures of 20-35 MPa. In two of the experiments, the sample was deformed at nominally dry conditions. In the third experiment, the sample was saturated with deionized water and deformed at a constant pore fluid pressure of 5 MPa under drained conditions. During the deformation tests, the maximum principal (compressive) stress σ_1 was increased in distinct steps of 1-5 MPa while the intermediate and minimum principal stresses, $\sigma_2 = \sigma_3 = 20 - 35$ MPa, were kept constant until macroscopic failure occurred (**Figure** 1). After each differential stress (σ_1 - σ_2) increase, we acquired a microtomographic scan of the deforming rock at in situ stress conditions. From these scans, we obtained the evolving three-dimensional (3D) fracture networks within the samples (**Figure** 2). **We developed novel methods of tracking the growth of fractures that enable distinguishing between fractures that grow via isolated propagation and those that grow from the coalescence of several fractures. These new methods enable quantitatively comparing the competing influences of 1) nucleation and preexisting propagation, 2) isolated propagation and coalescence, and 3) local stress perturbations. Our analyses show that these competitions evolve toward macroscopic failure and depend on the stress states and interstitial fluid.**

2. Methods

2.1. In situ X-ray tomography

We performed three triaxial deformation experiments with in situ dynamic X-ray synchrotron microtomography at beamline ID19 at the European Synchrotron and Radiation Facility (ESRF). We deformed monzonite cylinders 1 cm in height and 0.4 cm in diameter **using the HADES apparatus (*Renard et al*., 2016). Monzonite is an igneous crystalline rock with**

similar mechanical properties to granite. Using the porosity measured in the tomograms, the initial porosity of each rock core is close to zero. This monzonite has a mean grain size of 450 µm (*Aben et al*., 2016). The large grain size relative to the sample size may cause the representative elementary volume (REV) of the system to approach the size of the sample. The question of the appropriate REV size is critical to address in order to aid reproducibility of the results, but difficult to estimate. Whether or not a REV exists depends on the rheology: for elastic materials it may exist, but for softening materials it may not (*Gitman et al*., 2007). Due to the large grain size relative to the sample size, we are above the minimum limit of a REV in granular materials (10 grains), and below the upper limit for stick-slip phenomena with glass beads (10^7) (*Evesque & Adjemian*, 2002). The following analysis, and previous work describing these experiments (*Renard et al*., 2018, 2019b), find general similarities in fracture network development in these three experiments, suggesting the reproducibility and robustness of the results.

In each experiment, we imposed a constant confining pressure ($\sigma_2 = \sigma_3$) and then increased the axial stress (σ_1) in steps until the rock failed macroscopically (**Figure** 1). After each differential stress increment, we acquired a scan of the sample at in situ stress conditions with **6.5 µm voxel resolution** (*Renard et al*., 2016). The duration of each scan is within 2 minutes. The experiments were conducted at room temperature, at three different confining pressures: 20 MPa (experiment #3), 25 MPa (#5), and 35 MPa (#4). Macroscopic failure occurred in a sudden stress drop. The final scan was taken at a differential stress very close to the failure stress, typically <0.5 MPa below the failure stress. Experiments #3 and #5 were conducted at nominally dry conditions, while the sample was fully saturated in experiment #4. **This sample was submerged in deionized water for 24 hours under vacuum before the experiment to help ensure that the pore space was saturated.** In experiment #4, a constant pore fluid pressure of 5 MPa was maintained using two pore pressure pumps connected at each end of the sample (top and bottom). Experiment #4 is also unique in that we reached the axial stress limit of the device (200 MPa) preceding macroscopic failure, and thus we reduced the confining pressure in steps of 1 MPa from 35 to 31 MPa until the core failed. Consequently, the sample experienced 35 MPa of confining pressure for 60 scans and stress steps, and then experienced 34 MPa, 33 MPa, 32 MPa, and 31 MPa confining pressure in the final four scans preceding failure, respectively. *Renard et al*. (2018, 2019b) describe the experimental conditions in further detail. ***Renard et al.* (2018) describe experiments #3 and #4. *Renard et al.* (2019b) analyze experiment #5. In the present study, we develop a new technique to follow the dynamics of fracture growth by categorizing this growth into three endmember modes of growth**. The X-ray tomography data of the three experiments are publicly available (*Renard*, 2017, 2018).

2.2. Extraction of the fracture networks

From the time series of 3D adsorption coefficient fields acquired throughout loading, we identify fractures and pores using a standard thresholding technique. The histogram of grey-scale values from a tomogram of a porous rock tends to have two maxima indicative of the modes of the solid and air (or deionized water) populations, respectively (e.g., *Renard et al*., 2019a). The local minimum of this histogram then determines the threshold that indicates whether voxels are identified as pore space or solid. Segmenting the tomograms with this procedure yield 3D binary fields of zeros and ones that indicate whether a voxel is within or outside of a fracture or pore. Because we employ the same threshold throughout loading in each experiment, the choice of the threshold has a similar effect for the entire time series of scans.

From the binary field, we extract individual fracture or pore objects by identifying groups of voxels that have 26-fold connectivity, the highest degree of connectivity in 3D. For each group of voxels, we calculate the covariance matrix and corresponding eigenvectors and eigenvalues, which describe the shape of each fracture using three principal orthogonal length scales corresponding to the eigenvectors. If the pore had an ellipsoidal shape, the three eigenvalues would represent the lengths of the three axes of the ellipsoid. We then use these eigenvalues to characterize the dimensions of fractures and pores in subsequent analyses. For all of the calculations using the fracture volume, we use the actual volume of the group of connected voxels. For all calculations that depend on the placement of the fractures in space, we use the three eigenvalues calculated from the covariance matrix. **Because mineral grain boundaries do not exert a significant impact on the geometry of fractures in these monzonite cores, the three eigenvectors of the covariance matrix provide a close approximation of the true fracture.**

2.3. Identifying nucleating, propagating and coalescing fractures

After identifying the individual fractures at each loading step of an experiment, we now track the fractures across several loading steps. In addition, we develop a method that links one or more fractures at the previous loading step (t_n) to the next loading step (t_{n+1}) (**Figure** 3). **This development is the central difference between this new method and the previous method of tracking fractures in X-ray tomography data developed by *Kandula et al.* (2019), and used in *McBeck et al.* (2019a).** The previous method did not allow linking more than one fracture in t_n to a fracture in t_{n+1}. Thus, *Kandula et al.* (2019) could identify when an individual fracture gained or lost volume from one loading step (and tomogram) to the next. However, this analysis could not differentiate between fractures that gained volume because one fracture propagated and opened, or because several fractures propagated and linked with each other (i.e., coalesced).

We developed this new method of tracking fractures in order to examine the competing influence of fracture coalescence and isolated propagation (**Figure** 3). Our method identifies one or more fractures in t_n and one fracture in t_{n+1} by searching for fractures in t_n that are within five voxels of a fracture in t_{n+1}. We use the ellipsoidal approximations of the fractures to do this search. The limit of five voxels helps ensure that the algorithm identifies fractures that have shifted in space due to deformation. The appropriate value of this limit may differ in rocks that experience differing axial and radial strains in each loading step to those observed here. We only perform the analysis for fractures with volumes >100 voxels. This volume threshold helps exclude noise from the analysis. The appropriate volume threshold is likely different for rocks that host differing ranges of fracture volumes than those observed here. Varying the volume threshold from 100 to 500 voxels does not change the main trends described in the results (**Figure** S1).

Determining whether a fracture is nucleating, propagation or coalescing at a given time step depends on the spatial resolution of the tomogram and the amount of opening that the fracture accommodates. We may only detect fractures

with apertures greater than the scan voxel size (6.5 µm). Thus, the nucleating classification refers to newly identified fractures with apertures > 6.5 µm, which may have formed in a previous loading step with apertures < 6.5 µm.

3. Results

3.1. Macroscopic mechanical behavior

The global mechanical behavior captured in the differential stress and axial strain relationships indicates that the monzonite samples undergo the deformation stages typical for brittle materials under triaxial compression (e.g., *Paterson & Wong*, 2005). We may separate the macroscopic deformation behavior into four different stages (**Figure** 1). Stage I is the initial non-linear stage corresponding to closure of preexisting defects. Stage II includes a quasi-linear relationship between stress and strain. Stage III occurs when deformation behavior deviates significantly from linearity. The yield point marks the boundary between stages II and III. Stage IV occurs shortly before macroscopic failure, when the effective elastic modulus is near zero (**Figure** 1). **Figure** 1 shows the axial strains when the initial shallowing occurs, which we refer to as the yield point in the subsequent text. We identify the yield point using the largest axial strain at which the difference between the observed differential stress and the differential stress predicted from a linear fit is less than 1% of the observed differential stress (**Figure** S2). We note that we leave the timing of the transitions from stage I to II and from stage III and IV as only qualitative in the subsequent analysis, while the transition from stage II to III is more precisely defined as the yield point. **The macroscopic failure of the rocks occurred in a sudden stress drop that either completely crushed the core (experiments #3 and #5), or allowed partial recovery of the core (#4). The macroscopic failure of experiment #4 included the formation of a system-spanning fracture network oriented approximately 30° from σ_1 (Figure 4 in *Renard et al*., 2018).**

3.2. Fracture nucleation and preexisting fracture propagation

Here we assess the dominance of fracture nucleation relative to the growth of preexisting fractures throughout loading in the three experiments (**Figure** 4). We track the number and total volume of fractures identified in a loading step that did (i.e., preexisting) and did not (i.e., nucleating) grow from a preexisting fracture identified in the previous loading step. In this and subsequent analyses, data reported for the time closest to macroscopic failure reflect the fracture network development that occurs from the second to last (t_{f-2}) and final (t_{f-1}) scan acquired in the experiment, where t_f is the time of macroscopic failure.

Throughout stages I-II in each experiment, both the number and total volume of preexisting and nucleating fractures increase with increasing strain at comparable levels (**Figure** 4). We consider the rate of growth as the increase in number or volume of fractures per strain increment. An increase/decrease in rate of growth thus marks an acceleration/deceleration in fracture growth in terms of number or volume. During the transition from stage II to III at yielding, the number and volume of the preexisting fractures accelerate, whereas the number and volume of nucleating fractures do not accelerate as quickly. Due to this bifurcation in acceleration, the number and volume of preexisting fractures exceed those of the nucleating fractures at the end of stage III and through stage IV, prior to failure (**Figure** 4a, b). At the end of stage IV, the volume of preexisting fractures exceeds the volume of newly nucleating fractures by several orders of magnitude (**Figure** 4b, c). In particular, at the end of stage VI the volume of newly nucleating fractures is 1%, <1%, and 13% of the volume of preexisting fractures in experiments #3, #5 and #4, respectively. **Overall, preexisting fracture propagation dominates fracture nucleation in the monzonite rocks deformed to failure.**

Our results show that while the acceleration in the number of preexisting fractures coincides with the yield point, the acceleration in the volume of preexisting fractures becomes significant only during stage IV, when macroscopic failure is imminent. This trend may also occur for the nucleating fractures, but the number of nucleating fractures identified near the yield point is too low to draw the conclusion with confidence. Finally, the function of preexisting fracture volume relative to axial strain is approximately constant in linear-log strain-volume space (**Figure** 4c), indicating an exponential increase in total volume as a function of axial strain. **The exponents of the best-fit exponential functions of the preexisting fracture volume relative to axial strain range from 725-2000 for the three experiments, with R^2 values between the best-fit functions and the data of 0.85-0.98.**

3.3. Isolated fracture propagation and fracture coalescence

To assess the influence of isolated fracture propagation relative to coalescence on fracture network development, we develop a method to recognize when fractures develop from the merger of two or more fractures (i.e., coalesce) or from the lengthening, opening or closing of only one fracture (i.e., isolated propagation). **Figure** 5 shows the number and total volume of fractures identified as developing from two or more fractures (i.e., coalescing) or from only one preexisting fracture (i.e., propagating). We use the short-hand term *propagating* to indicate fractures that grow in isolation, but we note that fractures identified as coalescing also propagate before or while they merge.

The number of propagating fractures is larger than the number of coalescing fractures throughout loading in each experiment (**Figure** 5a). The number and volume of the propagating fractures accelerate throughout stages II-IV. In contrast, the number and volume of the coalescing fractures only appear to accelerate following yielding, throughout stages III-IV. Overall, the differences in number and volume of propagating and coalescing fractures grow larger during stages I-III.

At the end of stage IV, immediately preceding macroscopic failure, the total volume of coalescing fractures exceeds the total volume of propagating fractures in the nominally dry experiments (experiments #3 and #5). During this stage, the volume of propagating fractures is 44% or 23% of the volume of coalescing fractures for experiments #3 and #5, respectively. In contrast, in the water-saturated experiment (#4), the total volume of coalescing fractures never exceeds the total volume of propagating fractures. Immediately preceding macroscopic failure, the volume of propagating fractures is about seven times higher than the volume of coalescing fractures in this experiment. **Thus, water-saturated conditions and higher confining stress appear to promote fracture propagation and suppress coalescence.**

3.4. Disperse and localized fracture growth

To characterize the influence of localization and stress perturbations on fracture network development, we identify the fractures that are gaining and losing volume from one loading step to the next, i.e., growing or closing, and whether they are located near or far from another fracture. **Analytical formulations of LEFM with the stress intensity factor suggest that fractures perturb their local stress field to a distance on the order of their length (e.g., *Chinnery & Petrak*, 1968; *Segall & Pollard*, 1980; *Atkinson*, 1987; *Scholz et al*., 1993; *Davy et al*., 2010, 2013). A corollary of this concept is that fractures that are within one fracture length of other (perturbing) fractures may be more likely to grow, and less likely to close.** This behavior will only be true if the local stress perturbation is favorable for growth. In contrast, local stress perturbations can also produce stress fields that hinder fracture growth, i.e., stress shadows. In this case, if a fracture lies in a stress shadow, it should be less likely to grow, and perhaps more likely to close. We test these inferences here. In particular, we track the number of growing and closing fractures that do (i.e., near) and do not (i.e., far) have other fractures within one fracture length of them at each stress step (**Figure** 6). For example, if one fracture (fracture #1) is located within y distance of another fracture (#2) with length y, then fracture #1 is counted in the *near* category.

The number of growing fractures matches the number of closing fractures in stages I-II early in loading (**Figure** 6a). During stage III after yielding, the number of growing fractures accelerates while the number of closing fractures remains at similar values. The number of growing fractures that are located near other fractures (within a fracture length of them) increases with loading (**Figure** 6b). In contrast, the number of growing fractures that are far from other fractures remains roughly constant throughout loading. These varying trends produce two patterns of fracture growth before and after the yield point. In stages I-II before yielding, the number of growing fractures located far from other fractures exceeds or is similar to the number of growing fractures located near other fractures. **These observations suggest that fractures located closer to other fractures are not more likely to grow than fractures spread further apart, indicating that stress concentrations produced by developing fractures do not appreciably influence fracture development preceding yielding**. In stages III-IV after yielding, however, the number of growing fractures located near to other fractures increasingly exceeds the number of growing fractures located far from other fractures. At the end of stage IV immediately preceding macroscopic failure in all three experiments, the number of growing fractures located near to others is 3-5 times higher than the number growing far from others. **When macroscopic failure becomes imminent, the stress concentrations produced by growing fractures appear to promote growth rather than suppress it.**

The evolution of the number of growing fractures located near to others further highlights the influence of coalescence on fracture network development (**Figure** 6b). The number of these fractures decreases in the final loading steps just before failure in the dry experiments (#3 and #5). In contrast, the number of these fractures continually increases in the water-saturated experiment (#4). Fracture coalescence reduces the total number of fractures as many smaller fractures merge into a few larger fractures.

4. Discussion

4.1. The competition between fracture nucleation and preexisting fracture propagation

In these monzonite rocks undergoing brittle failure, preexisting fracture propagation dominates fracture nucleation after yielding (**Figure** 4). At a macroscopic scale, many of the conditions that favor fracture nucleation also favor preexisting propagation, such as higher differential stress and/or lower effective confinement. **At a more local scale, mechanical heterogeneities control the location of fracture nucleation and the growth of preexisting fractures. For example, *Tapponnier & Brace* (1976) documented that fracture development initiates along grain boundaries and healed transgranular fractures in granite, and new transgranular fractures propagate only at higher differential stresses**. In granular cohesive rocks, such as sandstone, shear and/or tensile stress concentrations at the boundary of grains can also promote fracture nucleation (e.g., *Menéndez et al*., 1996; *Baud et al*., 2004; *Zhu et al*., 2010). These mechanical controls influence the ability of fractures to nucleate and propagate following nucleation: fractures can arrest at grain boundaries and mechanical contacts, depending on the degree of stress transfer across such interfaces (e.g., ***Tapponnier & Brace*, 1976**; *Cooke & Underwood*, 2001; *McBeck et al.,* 2019a, b). Thus, the competing influence of these modes of fracture network development (nucleation or preexisting propagation) is difficult to predict in rocks that include such mechanical heterogeneities, and may be more challenging in rocks without such strong heterogeneities, such as monzonite. **Granular rocks may contain mechanical heterogeneities that concentrate shear and/or tensile stresses more effectively than monzonite, which consists of an interlocking crystalline structure with more homogeneous mechanical properties.** For example, numerical discrete element method models of sandstone indicate that the degree of strength heterogeneity between grain boundaries and intragranular material controls the proportion of fractures that nucleate at grain boundaries and those that nucleate within grains (*McBeck et al.,* 2019b). Thus, in a given sandstone volume there will likely be a greater number of sites of significant stress concentrations than in a monzonite or granite volume, and thereby a larger number of sites suitable for fracture nucleation. **Consequently, we may expect a greater dominance of nucleation in sandstone and other rocks with strong strength heterogeneity than observed in these monzonite rocks.**

In the crust, interfaces between mechanical sequences can exert a first order effect on the extent of fracture propagation. In sedimentary volumes consisting of parallel layers, for example, mechanical interfaces can arrest fracture growth (e.g., *Cooke & Underwood*, 2001; *Underwood et al*., 2003). When these interfaces hinder growth in sedimentary sequences undergoing layer-parallel extension, the competition between fracture nucleation and propagation follows a systematic evolution. In these systems, new fractures nucleate, propagate perpendicular to the maximum tensile direction, open parallel to this direction, and (sometimes) arrest their propagation at an interface so that eventually the spacing between fractures is proportional to the layer thickness (e.g., *Narr & Suppe*, 1991). When the spacing between fractures reaches a certain critical value, the layer becomes saturated such that no (or few) fractures nucleate and only the preexisting fractures open in order to accommodate the applied extension (e.g., *Wu & Pollard*, 1995; *Zheng et al*., 2019). **Thus, early in loading fracture nucleation dominates, and later in loading preexisting fracture development dominates.**

Here, we document how the competition between fracture nucleation and preexisting development evolves with increasing differential stress in triaxial compression (e.g., **Figure** 7), similar to the evolution observed in extending layered sedimentary sequences. Our results indicate that increasing differential stress promotes the dominance of preexisting fracture development rather than nucleation. As the fractures lengthen and open under increasing differential stress, the stress intensity factors at their tips increase (*Isida*, 1971) and thereby further promote propagation. As deformation localizes among several larger fractures, the energetic cost of propagating preexisting fractures may become less than the cost of nucleating new fractures (e.g., *Del Castello & Cooke*, 2007; *Herbert et al*., 2015). Our data support these predictions from the linear elastic fracture mechanics and energy optimization.

4.2. The competition between isolated fracture propagation and coalescence

Tracking the volume of fractures that coalesce from several fractures and those that propagate in isolation without merging indicates that isolated propagation dominates coalescence throughout most of the deformation process preceding macroscopic failure (**Figure** 5). Preceding macroscopic failure, our results suggest that the presence of fluid and magnitude of confining stress may affect the competition between isolated propagation and coalescence. We deformed the water-saturated sample (experiment #4) with the highest effective confining stress; the confining pressure minus pore fluid pressure was 30 MPa. In this experiment, the total volume of coalescing fractures was <10% of the volume of propagating fractures immediately preceding macroscopic failure (**Figure** 5b). In contrast, in the experiments deformed at lower confining stress (20 and 25 MPa in experiments #3 and #5, respectively) and dry-conditions, the total volume of coalescing fractures was at least twice the volume of the propagating fractures preceding failure. This difference in behavior suggests that dry conditions and lower confining stress promote coalescence rather than isolated propagation.

Many observations indicate that the magnitude of confining stress influences fracture development. In the endmember case when a rock undergoes uniaxial compression (i.e., zero confinement), experiments show that opening mode and tensile failure dominate deformation with little evidence of shear deformation (e.g., *Lin et al*., 2015). ***Tapponnier & Brace* (1976) observed few shear fractures in triaxial experiments on Westerly granite under 50 MPa confining stress.** With increasing confinement, fractures can appear to rotate from the orientation preferred under uniaxial compression conditions (parallel to the maximum compression direction), toward the range of orientations predicted by the maximum Coulomb shear stress (e.g., *Mair et al*., 2002; *McBeck et al*., 2019a). Analyses often interpret such rotation to indicate an increasing dominance of shear deformation at the expense of tensile deformation. However, such apparent rotation may occur as many individual mode-I fractures link together so that the macroscopic trend of the fault is inclined relative to the maximum compression direction (e.g., *Peng & Johnson*, 1972; *Lockner et al*., 1991; *Renard et al*., 2019a). Consequently, the fracture geometry alone may not indicate the relative proportion of shear and tensile deformation.

Analysis of the moment tensors of acoustic emissions provides further insights to the relative proportion of shear and tensile deformation under varying confining stresses. Analysis of acoustic emissions during triaxial compression suggests that decreasing confining stress promotes tensile failure and opening at the expense of shear failure (e.g., *Stanchits et al*., 2006).

This opening may enable greater access to preexisting fractures than shear deformation, thereby promoting the likelihood of coalescence. For example, mixed-mode fractures may tend to have larger apertures than fractures dominated by shear deformation. Consequently, mixed-mode failure may result in thicker fractures that provide greater surface area to which other fractures can link than thinner fractures produced predominately by shear. The presence of damage zones surrounding crustal faults and the decreasing of the thickness of such damage zones with depth (e.g., *Harding*, 1985) support the idea that confining stress localizes deformation in low porosity crystalline rock. Confining stress tends to reduce the proportion of tensile deformation relative to shear deformation, and thus may localize deformation into thinner zones, in the absence of cataclastic flow and ductile deformation.

The applied confining pressure in experiment #5 was 5 MPa higher than that of experiment #3, but these two dry samples show similar proportions of fracture propagation and coalescence. Consequently, it is unlikely that the 5 MPa higher effective stress of experiment #4 compared to experiment #5 is the primary trigger of the different behaviors observed in these experiments. We suggest that the presence of water is responsible for the transition from isolated propagation to coalescence-dominated fracture network development. **We acknowledge that this conclusion rests on only three experiments and further work is required for more robust support of this idea. However, previous work focused on the influence of water on fracture network growth supports this idea. In particular, this work shows that chemical reactions at fracture tips can influence fracture propagation.** Such stress corrosion cracking occurs when chemical reactions reduce the fracture toughness and thereby promote crack propagation (e.g., *Anderson & Grew*, 1977). When water is present, hydrogen bond formation weakens the Si-O bond in quartz-rich sandstones, producing water-weakening (e.g., *Baud et al*., 2000). Stress corrosion cracking may thus promote nucleation at the expense of coalescence in the water-saturated monzonite experiment.

Changes in pore fluid pressure can also affect the fracture propagation rate (*Ougier-Simonin & Zhu*, 2013, 2015). Recent studies show that at the same effective pressure and loading, fault propagation in intact serpentinite is slower in samples with higher pore fluid pressures (*French & Zhu*, 2017). When a fluid-saturated rock dilates, the pore pressure may drop and thereby reduce the local effective confinement and strengthen the rock, i.e., dilatant hardening (e.g., *Brace & Bombolakis*,1963; *Rice*, 1975; *Rudnicki & Chen*, 1988; *Ikari et al*., 2009; *Xing et al*., 2019; *Brantut*, 2020). This strengthening can then slow the rate of fracture propagation from dynamic to quasi-stable (***Martin*, 1980**; *French & Zhu*, 2017). Dilatant hardening can operate in intact rock as well as saturated gouge zones (*Ikari et al*., 2009; *Xing et al*., 2019). For example, increasing pore pressure causes the frictional behavior of antigorite gouge to evolve from velocity-weakening to velocity-strengthening (*Xing et al*., 2019). Dilatant hardening may influence fracture development in the water-saturated experiment (#4) **if the evolving permeability of the network is high enough to allow fluid flow at the time scale of the experiment**. **Using the porosity identified in the tomograms acquired immediately preceding failure, the porosity of the rocks in each experiment ranges from 0.06% (#4), 0.2% (#3), and 1.6% (#5) at this stage. Following the relationships between porosity and permeability calculated for dynamically fractured monzonite cores (*Aben et al*., 2020), rocks with 0.06-1.6% porosity may have permeability 10^{-16} to 10^{-18} m^{-2}. With this range of permeability and dimensions of the rock core, water requires about less than a minute to 45 minutes to traverse the core from top to bottom (Text S1). Thus, the time interval of the loading steps (3**

minutes) may allow water to flow between fractures, enabling the effects of stress corrosion cracking and dilatant hardening to operate at least in the final stages preceding failure. Earlier in the experiment, when the porosity and permeability is lower, the lower flow rate may suppress such effects. Further experimental investigations are needed to distinguish between the relative importance of stress corrosion cracking and dilatant hardening on fracture development within water-saturated rocks.

These observations and our analyses suggest that the presence of water (producing stress corrosion) and high pore fluid pressure (producing dilatant hardening) promote slower, more isolated fracture network growth, rather than faster, coalescence-dominated growth. Understanding the mechanical and chemical conditions that favor one mode of fracture growth over another (e.g., fracture coalescence versus isolated fracture propagation) has important implications in many energy and environmental engineering practices. For example, when their connected porosities are comparable, fracture networks produced by the propagation and coalescence of many small fractures may have lower connectivity, higher tortuosity and lower permeability than networks consisting of a few large fractures. However, the fracture networks consisting of numerous small fractures may be more efficient in shale gas exploration and CO_2 sequestration (e.g., *Xing et al*., 2018).

4.3. The influence of local stress perturbations on fracture growth

A clear factor in fracture network development is the fracture network density, clustering, or localization. For example, earthquakes are more likely to arrest at the ends of faults that are >5 km from another fault (*Wesnousky*, 2006). Indeed, the distance between fractures is one of the key parameters that predicts whether they grow or close from one stress step to the next in X-ray tomography triaxial compression experiments on marble, monzonite and granite rocks (*McBeck et al*., 2019a). Analytical solutions from LEFM provide a mechanical interpretation of these observations. These solutions indicate that a fracture will perturb the local stress field to a distance on the order of their length (e.g., *Scholz et al*., 1993). **Following this idea, we may use the number of growing fractures located within this threshold to another fracture to determine if stress perturbations produced by growing fractures tend to promote or hinder growth**.

Our observations suggest that local stress perturbations produced by growing fractures promote the growth of neighboring fractures during stages III-IV preceding macroscopic failure (**Figure** 6). During these stages, the number of fractures that grow and are located within one fracture length exceeds the number of fractures that grow and are located outside of this threshold. Preceding yielding, however, similar numbers of growing fractures are located both within and outside this threshold. When the fracture network is more diffuse under lower differential stress, the distance between fractures does not appear to influence whether a fracture grows or closes (i.e., **Figure** 7). When the fracture network becomes more clustered, the distance between fractures appears to influence whether a fracture grows or closes. Our results highlight the conditions under which stress perturbations influence growth in rocks under triaxial compression that host fracture networks with a variety of spatial distributions.

5. Conclusions

In situ dynamic X-ray tomography during the triaxial compression of crystalline rocks reveals the competing influence of three modes of fracture network development: 1) nucleation, 2) isolated propagation and 3) coalescence. We find that the influence of these modes evolves throughout loading, with clear transitions near yielding and macroscopic failure. Preexisting fracture propagation, including isolated propagation and coalescence, becomes the dominant mode of deformation following yielding. Coalescence then becomes the dominant mechanism of fracture network development in dry samples under lower confinements only immediately preceding macroscopic failure. Isolated propagation remains the dominant mechanism throughout loading in a water-saturated sample under higher confinement. Compared to the prediction that fractures promote growth by perturbing their local stress field to a distance on the order of their length (e.g., *Scholz et al.*, 1993), our observations only match these expectations in the stages of the experiments between yielding and macroscopic failure. Preceding yielding, however, the fractures that are growing are not significantly closer to other fractures, **indicating that their stress perturbations do not promote the growth of neighboring fractures**. **When the rock experiences lower differential stress and the fracture network is more distributed, 1) similar numbers of new fractures nucleate and preexisting fractures grow, 2) isolated propagation dominates coalescence, and 3) local stress perturbations do not appear to promote fracture growth (Figure** 7). **When the rock experiences higher differential stress following yielding, 1) preexisting fracture propagation dominates new fracture nucleation, 2) coalescing fracture volume exceeds the propagating fracture volume in dry samples when macroscopic failure is imminent, and 3) local stress perturbations promote fracture growth.**

Data availability. The data are available on the Norstore repository (*Renard*, 2017, 2018).

Author contributions. JM and FR performed the experiments, analyzed results, and wrote the manuscript. WZ analyzed results and wrote the manuscript.

Competing interests. There are no competing interests.

Acknowledgements. We thank Elodie Boller, Paul Tafforeau, and Alexander Rack for providing advice on the design of the tomography setup, Benoît Cordonnier for experimental expertise, and Sanchez Technology for building the deformation apparatus. The Research Council of Norway (awards 272217 to FR and 300435 to JM) and U.S. National Science Foundation (EAR-1761912 to WZ) funded this work. The European Synchrotron Radiation Facility allocated beamtime (Long Term Proposal ES-295). **We thank guest editor André Niemeijer, reviewer Frans Aben and an anonymous reviewer for suggestions that improved this manuscript.**

References

Aben, F. M., Brantut, N., Mitchell, T. M., and David, E. C.: Rupture Energetics in Crustal Rock From Laboratory-Scale Seismic Tomography. Geophysical Research Letters, 46(13), 7337-7344, 2019.

Aben, F. M., Doan, M.-L., and Mitchell, T. M.: Variation of hydraulic properties due to dynamic fracture damage: Implications for fault zones. Journal of Geophysical Research: Solid Earth, 125, e2019JB018919, 2020.

Aben, F. M., Doan, M. L., Mitchell, T. M., Toussaint, R., Reuschlé, T., Fondriest, M., Gratier J-P., and Renard, F.: Dynamic fracturing by successive coseismic loadings leads to pulverization in active fault zones. Journal of Geophysical Research: Solid Earth, 121(4), 2338-2360, 2016.

Anderson, O. L. and Grew, P. C.: Stress corrosion theory of crack propagation with applications to geophysics, Rev. Geophys. Space Phys.15, 77– 104, 1977.

Atkinson, B. K.: Subcritical crack growth in geological materials. Journal of Geophysical Research: Solid Earth, 89(B6), 4077-4114, 1984.

Atkinson, B. K.: Fracture Mechanics of Rock, 534, Academic, London, 1987.

Baud, P., Klein, E., and Wong, T. F.: Compaction localization in porous sandstones: spatial evolution of damage and acoustic emission activity. Journal of Structural Geology, 26(4), 603-624, 2004.

Baud, P., Zhu, W., Wong, T.-F.: Failure mode and weakening effect of water on sandstone. Journal of Geophysical Research, 105, 16,371-16,389, 2000.

Blanpied, M. L., Marone, C. J., Lockner, D. A., Byerlee, J. D., and King, D. P.: Quantitative measure of the variation in fault rheology due to fluid-rock interactions. Journal of Geophysical Research: Solid Earth, 103(B5), 9691-9712, 1998.

Brace, W. F., and Bombolakis, E. G.: A note on brittle crack growth in compression. Journal of Geophysical Research, 68(12), 3709–3713. doi:10.1029/JZ068i012p03709, 1963.

Brantut, N.: Dilatancy-induced fluid pressure drop during dynamic rupture: Direct experimental evidence and consequences for earthquake dynamics. Earth and Planetary Science Letters, 538, 116179, 2020.

Chinnery, M. A., and Petrak, J. A.: The dislocation fault model with a variable discontinuity, Tectonophysics, 5(6), 513–529, doi:10.1016/0040-1951(68)90008-5, 1968.

Cooke, M. L., and Underwood, C. A.: Fracture termination and step-over at bedding interfaces due to frictional slip and interface opening. Journal of Structural Geology, 23(2-3), 223-238, 2001.

Crider, J. G., and Peacock, D. C.: Initiation of brittle faults in the upper crust: a review of field observations. Journal of Structural Geology, 26(4), 691-707, 2004.

Cui, G., Wang, Y., Rui, Z., Chen, B., Ren, S., and Zhang, L.: Assessing the combined influence of fluid-rock interactions on reservoir properties and injectivity during CO2 storage in saline aquifers. Energy, 155, 281-296, 2018.

Davy, P., Goc, R., Darcel, C., Bour, O., Dreuzy, J., and Munier, R.: A likely universal model of fracture scaling and its consequence for crustal hydromechanics, Journal of Geophysical Research: Solid Earth, 115(B10), 1–13, doi:10.1029/2009jb007043, 2010.

Davy, P., Le Goc, R., and Darcel, C.: A model of fracture nucleation, growth and arrest, and consequences for fracture density and scaling, Journal of Geophysical Research: Solid Earth, 118, 1393–1407, doi:10.1002/jgrb.50120, 2013.

Del Castello, M., and Cooke, M. L.: Underthrusting-accretion cycle: Work budget as revealed by the boundary element method, Journal of Geophysical Research: Solid Earth, 112, B12404, doi:10.1029/2007JB004997, 2007.

Du, Y., and Aydin, A.: The maximum distortional strain energy density criterion for shear fracture propagation with applications to the growth paths of en echelon faults. Geophysical Research Letters, 20(11), 1091-1094, 1993.

Evesque, P., and Adjemian, F.: Stress fluctuations and macroscopic stick-slip in granular materials. The European Physical Journal E, 9(3), 253-259, 2002.

Fattaruso, L. A., Cooke, M. L., Dorsey, R. J., and Housen, B. A.: Response of deformation patterns to reorganization of the southern San Andreas fault system since ca. 1.5 Ma. Tectonophysics, 693, 474-488, 2016.

French, M. E., and Zhu, W.: Slow fault propagation in serpentinite under conditions of high pore fluid pressure. Earth and Planetary Science Letters, 473, 131-140, 2017.

Frery, E., Gratier, J. P., Ellouz-Zimmerman, N., Loiselet, C., Braun, J., Deschamps, P., Blamart, D., Hamelin, B., and Swennen, R., Evolution of fault permeability during episodic fluid circulation: Evidence for the effects of fluid–rock interactions from travertine studies (Utah–USA). Tectonophysics, 651, 121-137, 2015.

Gitman, I. M., Askes, H., and Sluys, L. J.: Representative volume: existence and size determination. Engineering fracture mechanics, 74(16), 2518-2534, 2007.

Griffith, A. A.: VI. The phenomena of rupture and flow in solids. Philosophical Transactions of the Royal Society of London. Series A, containing papers of a mathematical or physical character, 221(582-593), 163-198, 1921.

Harding, T. P.: Seismic characteristics and identification of negative flower structures, positive flower structures, and positive structural inversion. AAPG Bulletin, 69(4), 582-600, 1985.

Herbert, J. W., Cooke, M. L., Souloumiac, P., Madden, E. H., Mary, B. C., and Maillot, B.: The work of fault growth in laboratory sandbox experiments. Earth and Planetary Science Letters, 432, 95-102, 2015.

Hickman, S., Sibson, R., and Bruhn, R.: Introduction to special section: Mechanical involvement of fluids in faulting. Journal of Geophysical Research: Solid Earth, 100(B7), 12831-12840, 1995.

Ikari, M. J., Saffer, D. M., and Marone, C.: Frictional and hydrologic properties of clay-rich fault gouge. Journal of Geophysical Research-Solid Earth, 114, B05409, doi:10.1029/2008JB006089, 2009.

Irwin, G.: Analysis of stresses and strains near the end of a crack traversing a plate. Journal of Applied Mechanics 24, 361–364, 1957.

Isida, M.: Effect of width and length on stress intensity factors of internally cracked plates under various boundary conditions. International Journal of Fracture Mechanics, 7(3), 301-316, 1971.

Jackson, C. A. L., and Rotevatn, A.: 3D seismic analysis of the structure and evolution of a salt-influenced normal fault zone: a test of competing fault growth models. Journal of Structural Geology, 54, 215-234, 2013.

Jaeger, J. C., Cook, N. G. W., and Zimmerman, R.: Rock mechanics. Fundamentals of Rock Mechanics. Chapman and Hall, London, 1979.

Kandula, N., Cordonnier, B., Boller, E., Weiss, J., Dysthe, D. K., and Renard, F.: Dynamics of microscale precursors establish brittle-compressive failure as a critical phenomenon in Carrara marble. Journal of Geophysical Research, 124, 6121-6139, doi:10.1029/2019JB017381, 2019.

Kawakata, H., Cho, A., Yanagidani, T., and Shimada, M.: The observations of faulting in Westerly granite under triaxial compression by X-ray CT scan. International Journal of Rock Mechanics and Mining Sciences, 34(3-4), 151-e1–151-e12, 1997.

Lamy-Chappuis, B., Angus, D., Fisher, Q., Grattoni, C., and Yardley, B. W.: Rapid porosity and permeability changes of calcareous sandstone due to CO2-enriched brine injection. Geophysical Research Letters, 41(2), 399-406, 2014.

Lin, P., Wong, R. H., and Tang, C. A.: Experimental study of coalescence mechanisms and failure under uniaxial compression of granite containing multiple holes. International Journal of Rock Mechanics and Mining Sciences, 77, 313-327, 2015.

Lisabeth, H. and Zhu, W.: Effect of temperature and pore fluid on the strength of porous limestone. Journal of Geophysical Research, 120, 6191–6208, doi:10.1002/2015JB012152, 2015.

Lockner, D., Byerlee, J. D., Kuksenko, V., Ponomarev, A., and Sidorin, A.: Quasi-static fault growth and shear fracture energy in granite. Nature, 350(6313), 39-42, 1991.

Madden, E. H., Cooke, M. L., and McBeck, J.: Energy budget and propagation of faults via shearing and opening using work optimization. Journal of Geophysical Research: Solid Earth, 122(8), 6757-6772, 2017.

Mair, K., Elphick, S., and Main, I.: Influence of confining pressure on the mechanical and structural evolution of laboratory deformation bands. Geophysical Research Letters, 29(10), 49-1, 2002.

Mansfield, C., and Cartwright, J.: Fault growth by linkage: observations and implications from analogue models. Journal of Structural Geology, 23(5), 745-763, 2001.

Martin III, R. J.: Pore pressure stabilization of failure in Westerly granite. Geophysical Research Letters, 7(5), 404-406, 1980.

Martin, C. D., and Chandler, N. A.: The progressive fracture of Lac du Bonnet granite. International journal of rock mechanics and mining sciences & geomechanics abstracts, Vol. 31, No. 6, 643-659, Pergamon, 1994.

Mary, B. C. L., Maillot, B., and Leroy, Y. M.: Deterministic chaos in frictional wedges revealed by convergence analysis. International Journal for Numerical and Analytical Methods in Geomechanics, 37(17), 3036-3051, 2013.

McBeck, J., Cooke, M., and Fattaruso, L.: Predicting the propagation and interaction of frontal accretionary thrust faults with work optimization. Tectonophysics, 228461, 2020.

McBeck, J., Cooke, M., and Madden, E.: Work optimization predicts the evolution of extensional step overs within anisotropic host rock: Implications for the San Pablo Bay, CA. Tectonics, 36(11), 2630-2646, 2017.

McBeck, J., Kandula, N., Aiken, J. M., Cordonnier, B., and Renard, F.: Isolating the Factors That Govern Fracture Development in Rocks Throughout Dynamic In Situ X-Ray Tomography Experiments. Geophysical Research Letters, 46(20), 11127-11135, 2019a.

McBeck, J., Mair, K., and Renard, F.: How porosity controls macroscopic failure via propagating fractures and percolating force chains in porous granular rocks. Journal of Geophysical Research: Solid Earth, 124(9), 9920-9939, 2019b.

Menéndez, B., Zhu, W., and Wong, T. F.: Micromechanics of brittle faulting and cataclastic flow in Berea sandstone. Journal of Structural Geology, 18(1), 1-16, 1996.

Müller, G.: Starch columns: Analog model for basalt columns. Journal of Geophysical Research: Solid Earth, 103(B7), 15239-15253, 1998.

Narr, W., and Suppe, J.: Joint spacing in sedimentary rocks. Journal of Structural Geology, 13(9), 1037-1048, 1991.

Nemat-Nasser, S., & Horii, H.: Compression-induced nonplanar crack extension with application to splitting, exfoliation, and rockburst. Journal of Geophysical Research: Solid Earth, 87(B8), 6805-6821, 1982.

Okubo, C. H., and Schultz, R. A.: Evolution of damage zone geometry and intensity in porous sandstone: insight gained from strain energy density. Journal of the Geological Society, 162(6), 939-949, 2005.

Olson, J. E.: Joint pattern development: Effects of subcritical crack growth and mechanical crack interaction. Journal of Geophysical Research: Solid Earth, 98(B7), 12251-12265, 1993.

Olson, E. L., and Cooke, M. L.: Application of three fault growth criteria to the Puente Hills thrust system, Los Angeles, California, USA. Journal of Structural Geology, 27(10), 1765-1777, 2005.

Ougier-Simonin, A. and Zhu, W.: Effect of pore pressure build-up on slowness of rupture propagation. Journal of Geophysical Research, 120, 7966–7985, 10.1002/2015JB012047, 2015.

Ougier-Simonin, A. and Zhu, W.: Effects of pore fluid pressure on slip behaviors: an experimental study. Geophysical Research Letters, 40, 2619-2624, 10.1002/grl.50543, 2013.

Paterson, M. S., and Wong, T. F.: Experimental rock deformation-the brittle field. Springer Science and Business Media, 2005.

Peng, S., and Johnson, A. M.: Crack growth and faulting in cylindrical specimens of Chelmsford granite. In International Journal of Rock Mechanics and Mining Sciences and Geomechanics Abstracts (Vol. 9, No. 1, pp. 37-86). Pergamon, 1972.

Pollard, D. D., and Aydin, A.: Progress in understanding jointing over the past century. Geological Society of America Bulletin, 100(8), 1181-1204, 1988.

Reches, Z. E., and Lockner, D. A.: Nucleation and growth of faults in brittle rocks. Journal of Geophysical Research: Solid Earth, 99(B9), 18159-18173, 1994.

Renard, F.: Critical evolution of damage towards system size failure in a crystalline rock [Data set]. Norstore. doi:10.11582/2017.00025, 2017.

Renard, F.: Volumetric and shear processes in crystalline rock during the approach to faulting [Data set]. Norstore. doi:10.11582/2018.00023, 2018.

Renard, F., Cordonnier, B., Dysthe, D. K., Boller, E., Tafforeau, P., and Rack, A.: A deformation rig for synchrotron microtomography studies of geomaterials under conditions down to 10 km depth in the Earth. Journal of Synchrotron Radiation, 23(4), 1030-1034, 2016.

Renard, F., Gratier, J. P., and Jamtveit, B.: Kinetics of crack-sealing, intergranular pressure solution, and compaction around active faults. Journal of Structural Geology, 22(10), 1395-1407, 2000.

Renard, F., McBeck, J., Cordonnier, B., Zheng, X., Kandula, N., Sanchez, J. R., Kobchenko, M., Noiriel, C., Zhu, W., Meaken, P., and Fusseis, F.: Dynamic in situ three-dimensional imaging and digital volume correlation analysis to quantify strain localization and fracture coalescence in sandstone. Pure and Applied Geophysics, 176(3), 1083-1115, 2019a.

Renard, F., McBeck, J., Kandula, N., Cordonnier, B., Meakin, P., Ben-Zion, Y.: Volumetric and shear processes in crystalline rock approaching faulting. Proceedings of the National Academy of Sciences, 116, 16234-16239, doi: 10.1073/pnas.1902994116, 2019b.

Renard, F., Weiss, J., Mathiesen, J., Ben-Zion, Y., Kandula, N., and Cordonnier, B.: Critical evolution of damage toward system-size failure in crystalline rock. Journal of Geophysical Research: Solid Earth, 123(2), 1969-1986, 2018.

Rice, J. R.: On the stability of dilatant hardening for saturated rock masses. Journal of Geophysical Research, 80(11), 1531–1536. doi:10.1029/JB080i011p01531, 1975.

Rudnicki, J. W., and Chen, C. H.: Stabilization of rapid frictional slip on a weakening fault by dilatant hardening. Journal of Geophysical Research, 93(B5), 4745–4757. doi:10.1029/JB093iB05p04745, 1988.

Saeedi, A., Delle Piane, C., Esteban, L., and Xie, Q.: Flood characteristic and fluid rock interactions of a supercritical CO2, brine, rock system: South West Hub, Western Australia. International Journal of Greenhouse Gas Control, 54, 309-321, 2016.

Sausse, J., Jacquot, E., Fritz, B., Leroy, J., and Lespinasse, M.: Evolution of crack permeability during fluid–rock interaction. Example of the Brezouard granite (Vosges, France). Tectonophysics, 336(1-4), 199-214, 2001.

Scholz, C. H., Dawers, N. H., Yu, J. Z., Anders, M. H., and Cowie, P. A.: Fault growth and fault scaling laws: preliminary results. Journal of Geophysical Research: Solid Earth, 98(B12), 21951-21961, 1993.

Segall, P., and Pollard, D. D.: Mechanics of discontinuous faults. Journal of Geophysical Research, 85, 4337–4350, doi:10.1029/JB085iB08p04337, 1980.

Stanchits, S., Vinciguerra, S., and Dresen, G.: Ultrasonic velocities, acoustic emission characteristics and crack damage of basalt and granite. Pure and Applied Geophysics, 163(5-6), 975-994, 2006.

Tapponnier, P., and Brace, W. F.: Development of stress-induced microcracks in Westerly granite. International Journal of Rock Mechanics and Mining Sciences & Geomechanics Abstracts, Vol. 13, No. 4, 103-112, Pergamon, 1976.

Tenthorey, E., Cox, S. F., and Todd, H. F.: Evolution of strength recovery and permeability during fluid–rock reaction in experimental fault zones. Earth and Planetary Science Letters, 206(1-2), 161-172, 2003.

Underwood, C. A., Cooke, M. L., Simo, J. A., and Muldoon, M. A.: Stratigraphic controls on vertical fracture patterns in Silurian dolomite, northeastern Wisconsin. AAPG Bulletin, 87(1), 121-142, 2003.

Wesnousky, S. G.: Predicting the endpoints of earthquake ruptures. Nature, 444(7117), 358-360, 2006.

Wong, T. F., David, C., and Zhu, W.: The transition from brittle faulting to cataclastic flow in porous sandstones: Mechanical deformation. Journal of Geophysical Research: Solid Earth, *102*(B2), 3009-3025, 1997.

Wu, H., and Pollard, D.D.: An experimental study of the relationship between joint spacing and layer thickness. Journal of Structural Geology, 17(6), 887-905, 1995.

Xing, T., Zhu, W., French, M., and Belzer, B.: Stabilizing Effect of High Pore Fluid Pressure on Slip Behaviors of Gouge-bearing Faults. Journal of Geophysical Research: Solid Earth, 124(9), 9526-9545, 2019.

Xing, T., Zhu, W., Fusseis, F., and Lisabeth, H.: Generating porosity during olivine carbonation via dissolution channels and expansion cracks, Solid Earth, doi:10.5194/se-9-879-2018, 2018.

Zheng, X., Cordonnier, B., McBeck, J., Boller, E., Jamtveit, B., Zhu, W., and Renard, F.: Mixed-mode strain localization generated by hydration reaction at crustal conditions. Journal of Geophysical Research: Solid Earth, 124, 2019.

Zhu, W., Baud, P. and Wong, T.F.: Micromechanics of cataclastic pore collapse in limestone. Journal of Geophysical Research: Solid Earth, 115(B4), doi:10.1029/2009JB006610, 2010.

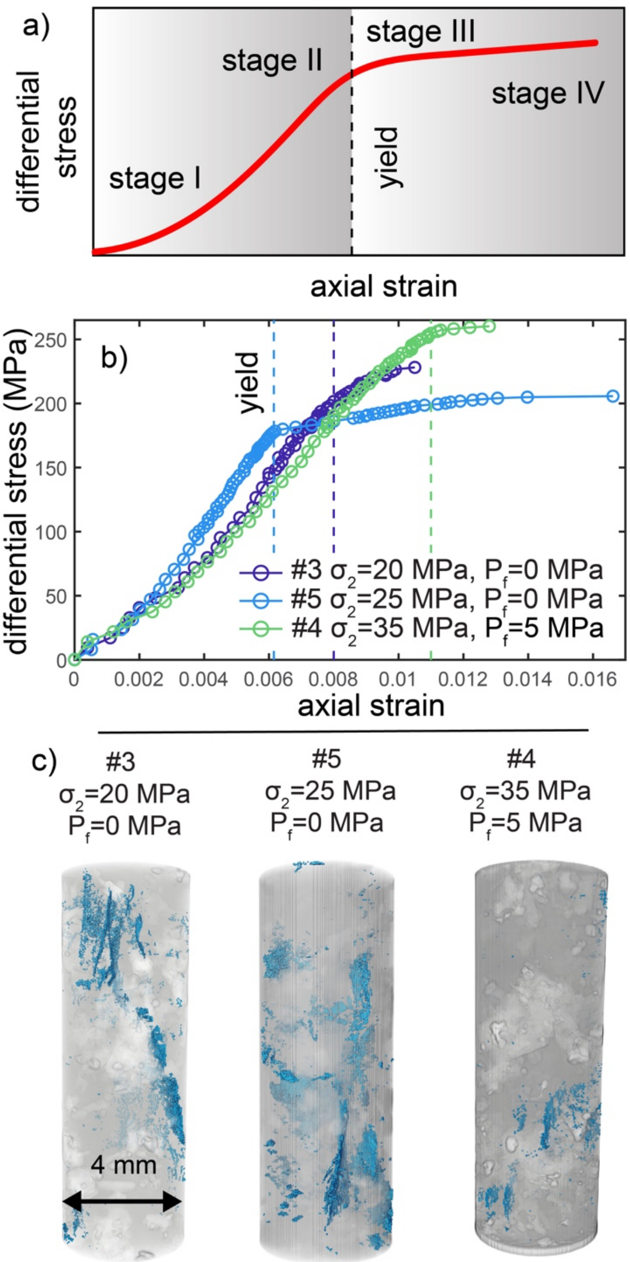

Figure 1: Macroscopic behavior of each experiment produced by fracture network development. a) Macroscopic stages of deformation. Stage I is the initial non-linear stage corresponding to the closure of preexisting defects. Stage II includes the quasi-linear relationship between stress and strain. Stage III occurs when deformation behavior deviates significantly from linearity. The yield point marks the boundary between stages II and III. Stage IV occurs close to macroscopic failure, when the effective elastic modulus is near zero. The timing of the transition between stages I-II, and stages III-IV remains approximate in this analysis. b) Differential stress and axial strain relationships of the three experiments: #3, #4, and #5. Circles show the conditions when a tomogram was acquired. The applied confining stress and pore fluid pressure increase from monzonite #3 ($\sigma_2 = 20\ MPa, P_f = 0$), #5 ($\sigma_2 = 25\ MPa, P_f = 0$) and #4 ($\sigma_2 = 35\ MPa, P_f = 5\ MPa$). c) Fracture geometry in the final scan in all three experiments. Fractures shown in blue, minerals shown with transparent grey and white. The fracture network geometry in the last scan acquired before macroscopic failure includes longer, more volumetric, and more connected fractures in the experiments with $\sigma_2 = 20 - 25\ MPa$ and $P_f = 0$ (#3, #5) than in the experiment with $\sigma_2 = 35\ MPa, P_f = 5\ MPa$ (#4).

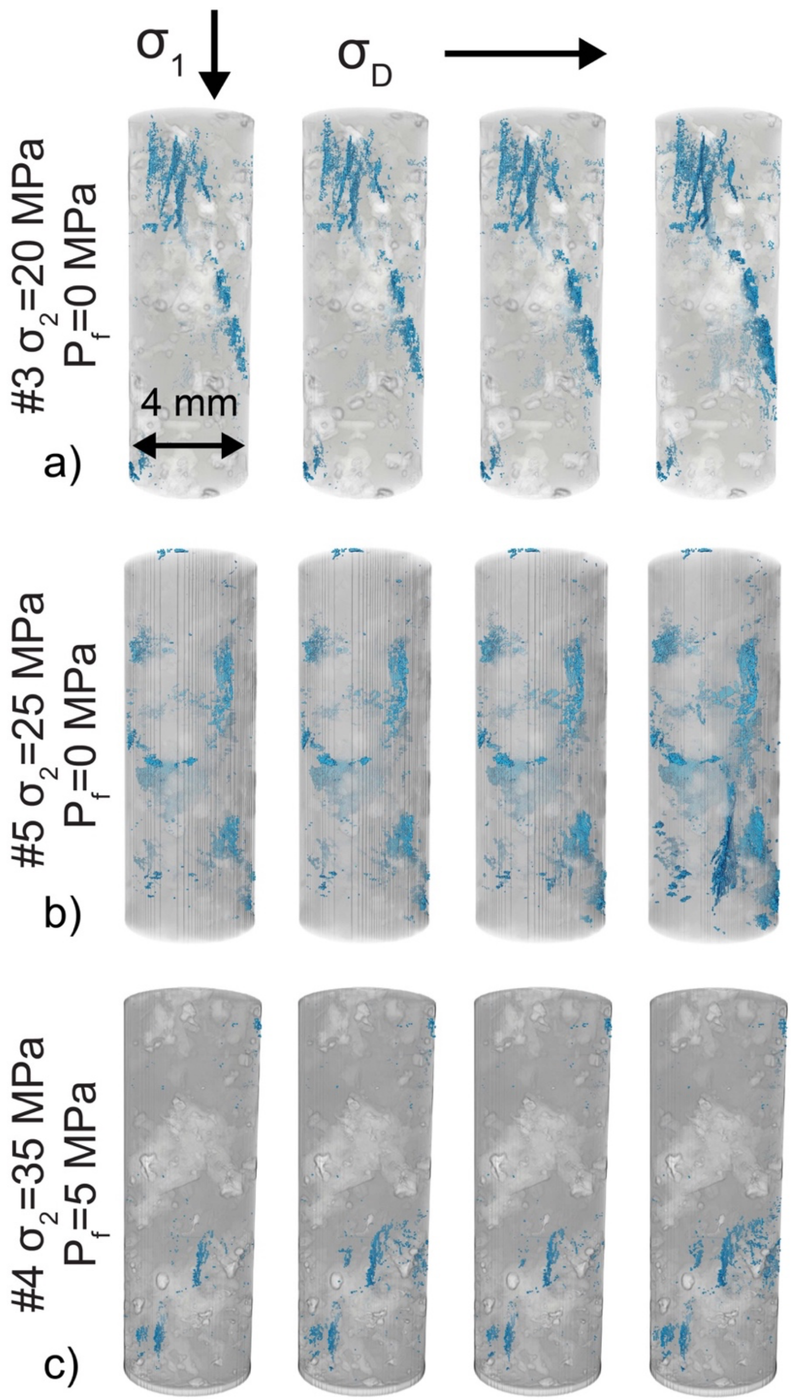

Figure 2: Evolving fracture networks in the final four loading steps of each experiment before system-size failure.

620

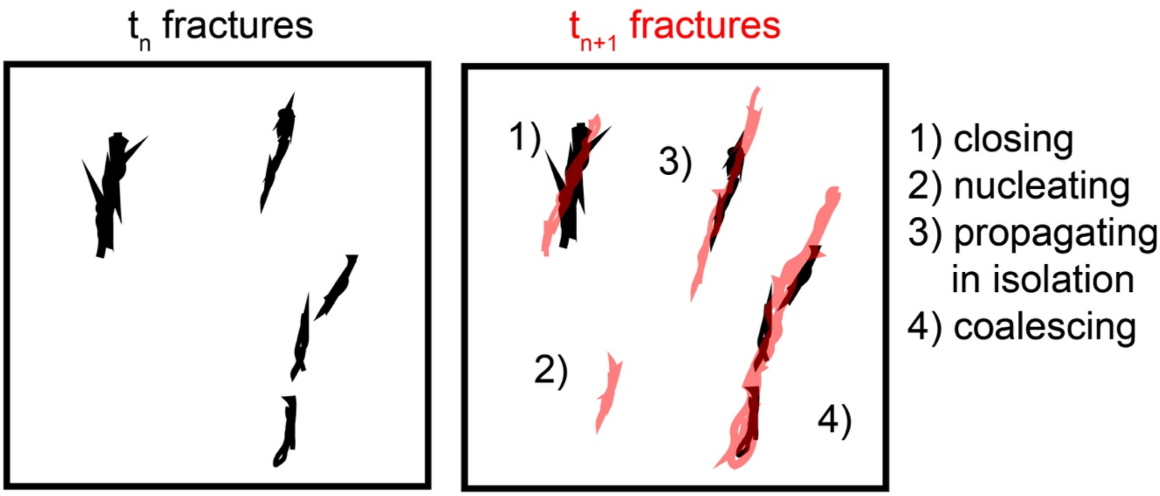

Figure 3: Modes of fracture network development captured by algorithm. By tracking individual fractures in sequential scans, we can identify fractures that 1) close, 2) nucleate, 3) propagate in isolation and 4) coalesce from one time to the next, t_n to t_{n+1}.

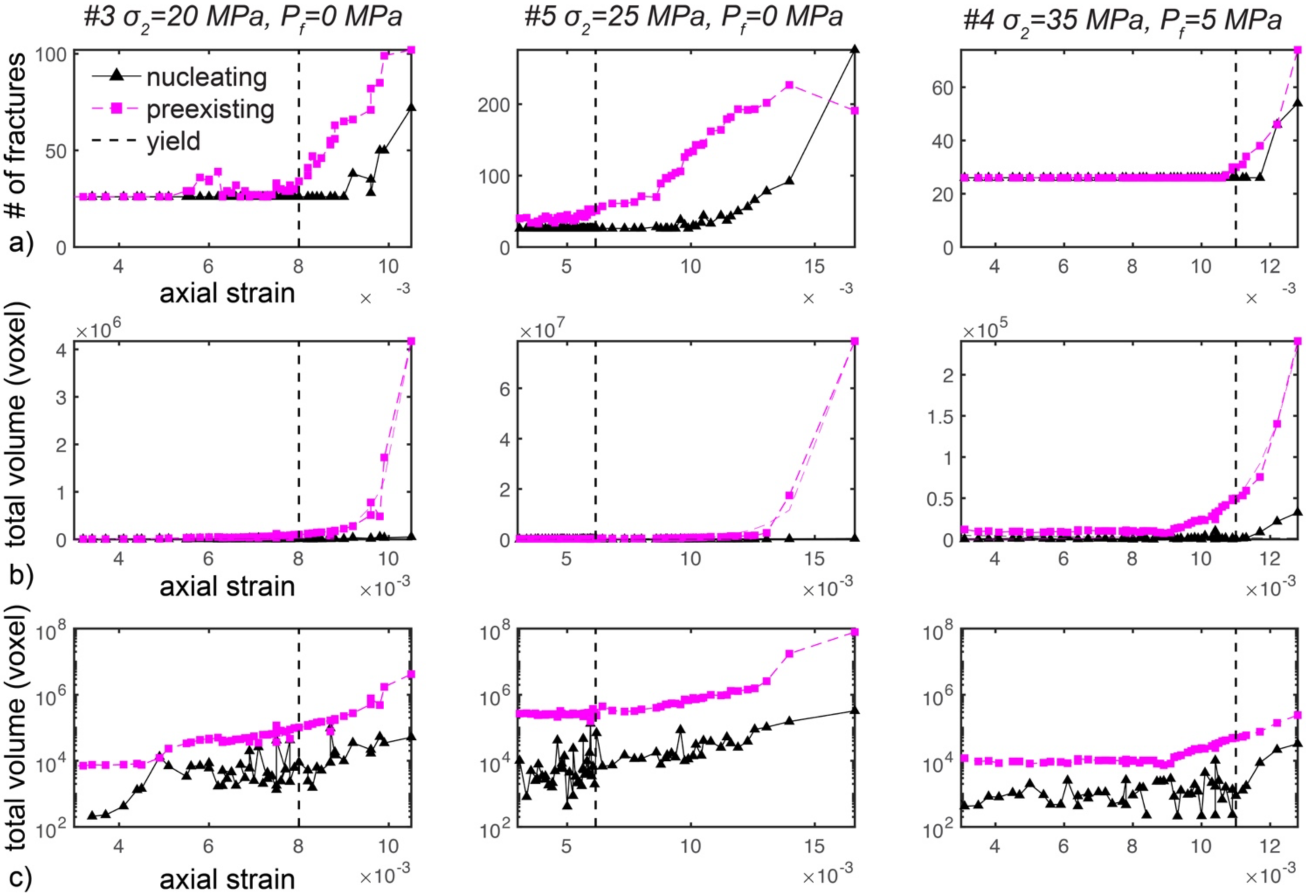

Figure 4: The competing influence of fracture nucleation and preexisting growth in each experiment. The applied effective pressure ($\sigma_2 - P_f$) increases from left to right. a) The number of fractures identified as nucleating or preexisting in each loading step. The total volume of the nucleating and preexisting fractures in linear b) and log-linear c) space. Dashed vertical lines show the axial strain at the macroscopic yielding point identified from the shallowing of the stress-strain curves (Figures 1, S2), separating stages I-II and III-IV. The pink lines without markers (b) show the best-fit exponential functions of the data. The total volume of preexisting fractures exceeds the volume of newly nucleating fractures in the final loading steps preceding macroscopic failure, indicating the dominance of preexisting development rather than nucleation. The increase of the volume of nucleating fractures after yield is more significant in the water-saturated sample compared to the nominally dry samples.

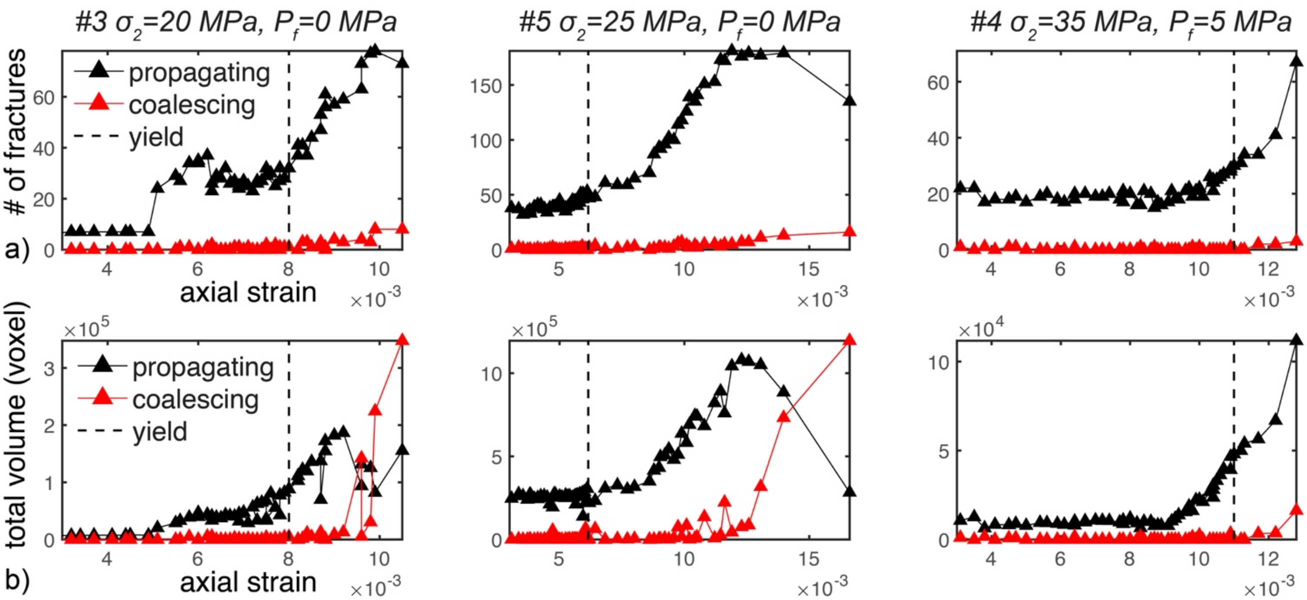

Figure 5: The varying influence of preexisting fracture coalescence and propagation. a) The number of fractures propagating in isolation (black) and coalescing (red). b) The total volume of fractures propagating in isolation or coalescing. Prior to macroscopic failure, the total volume of propagating fractures decreases and the total volume of coalescing fractures increases in the nominally dry experiments (#3 and #5), indicating the dominance of coalescence rather than isolated propagation. In contrast, in the water-saturated experiments, the propagating fractures dominate throughout loading.

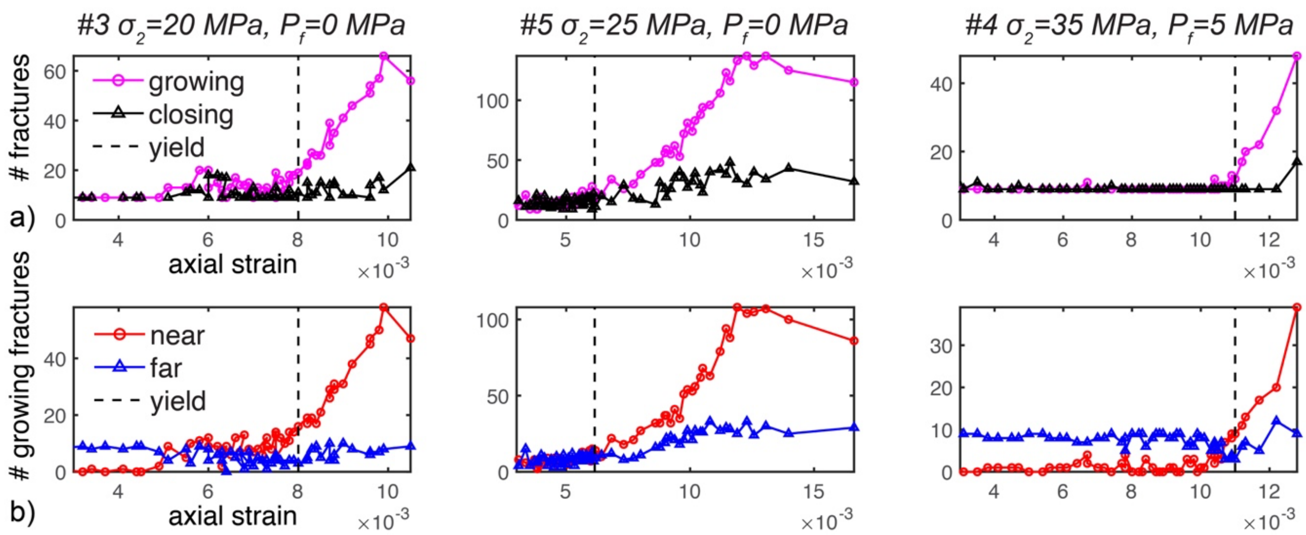

Figure 6: The influence of stress perturbations on fracture growth. a) The number of growing (magenta circles) and closing (black triangles) fractures. b) The number of growing fractures that do (*near*, red circles) and do not (*far*, blue triangles) have other fractures within one fracture length of them throughout loading. If one fracture (fracture #1) is located within *y* distance of another fracture (#2) with length *y*, then fracture #1 is counted in the *near* category. Following the macroscopic yield point, the number of growing fractures located near to other fractures exceeds the number located far from others. This observation suggests that the local perturbations of the stress field produced by fracture growth tend to promote the growth of other fractures following yielding.

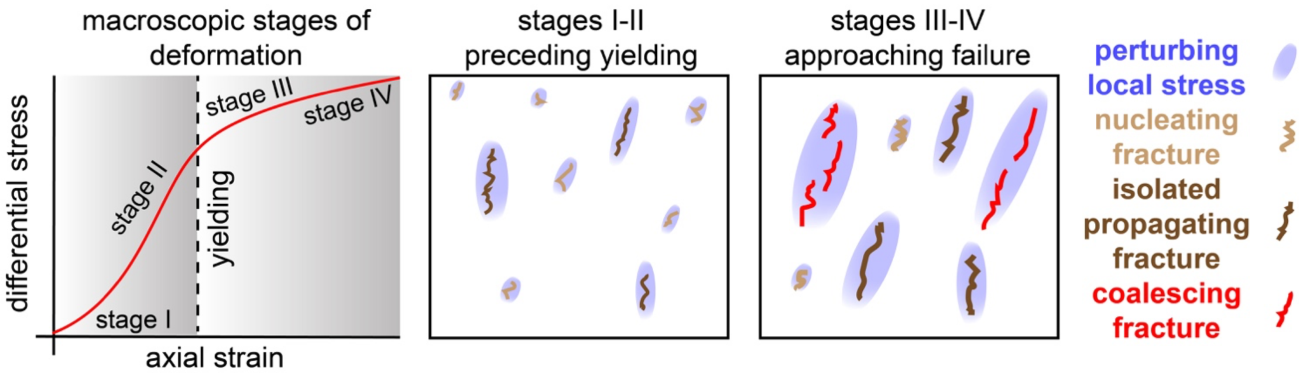

Figure 7: Schematic of varying modes of fracture development observed preceding yielding and approaching macroscopic failure. Nucleating, propagating, and coalescing fractures shown in light brown, dark brown and red, respectively. Blue ellipsoids show the approximate extent of the perturbation of the local stress field produced by fracture network development. When the rock experiences lower differential stress and the fracture network is more distributed, 1) similar numbers of new fractures nucleate and preexisting fractures grow, 2) isolated propagation dominates coalescence, and 3) local stress perturbations do not appear to promote fracture growth. When the system approaches macroscopic failure, 1) preexisting fracture propagation dominates new fracture nucleation, 2) coalescence dominates isolated propagation in the experiments with the lowest confining stress and dry conditions, and 3) local stress perturbations promote fracture growth.